*Sensors and Materials*, Vol. 38, No. 4 (2026) 1909–1923
MYU Tokyo



S & M 4415

# A Multisensor Fusion Framework for Collaborative robot Copper-Tube Brazing Application: Integrated Position Tracking and Quality Inspection Using Deep Learning Approach

Eugene Kim,[1†] Hwanhee Kang,[2†] Myeongjin Kim,[1]
Hyunrok Cha,[1] and Younggon Kim[1*]

[1]Purpose-Built Mobility Group, Seonam Division, Korea Institute of Industrial Technology, Gwangju 600-6114, Republic of Korea
[2]Robot Engineering, Korea National University of Science and Technology, 217 Gajeong-ro, Yuseong-gu, Daejeon 34113, Republic of Korea

(Received October 16, 2025; accepted January 15, 2026)

***Keywords:*** sensor fusion, image signal processing, RGB-thermal vision, deep learning classification, welding quality

In this study, the authors propose an integrated sensor-based framework consisting of two core components: a robot control module and a welding quality inspection module. The proposed system relies on vision sensors to acquire real-time visual information from the brazing process. For robot control, image-based sensing using a vision sensor and You Only Look Once-based object detection are performed to enhance positional accuracy and adaptability during autonomous brazing processes. For quality assessment, a convolutional neural network combined with a temporal attention mechanism is utilized to capture both spatial and temporal characteristics of the welding process, enabling the robust classification of weld quality. Experimental results demonstrate that the proposed approach achieves an $F1$-score of 98% under target manufacturing conditions. These findings highlight the potential of deep-learning-based vision and attention mechanisms for improving process reliability and automation in intelligent manufacturing environments.

## 1. Introduction

Recent advances in AI have accelerated innovation in autonomous manufacturing, particularly in the home appliance industry where smart factories are becoming increasingly prevalent.[1,2] The traditional paradigm of automation has evolved into autonomous manufacturing, characterized by self-adaptive systems capable of decision-making and process optimization. This transition marks the emergence of Physical AI, where intelligent algorithms directly interact with and control physical processes.[3–5] Among the various stages of appliance

*Corresponding author: e-mail: ygkim1@kitech.re.kr
†Eugene Kim and Hwanhee Kang contributed equally to this work.
https://doi.org/10.18494/SAM5983

ISSN 0914-4935 
https://myukk.org/

production, welding processes have drawn particular attention owing to their decisive effect on product durability and the complexity of ensuring consistent weld quality.[6,7]

Recent studies have explored AI-based approaches for welding process monitoring, defect detection, and quality evaluation. Many of these works employ deep learning models such as convolutional neural networks (CNNs) and object detection algorithms to identify weld defects from images or videos.[8–11] For instance, several researchers have demonstrated that vision-based systems can outperform traditional sensor-based inspection methods in identifying surface defects.[12–14] Others have proposed hybrid models combining thermal or acoustic data with visual inputs to enhance detection accuracy.[15–17] However, despite these advances, relatively few studies have addressed the integration of intelligent vision systems with robotic control, especially concerning the optimal placement of sensors and real-time system integration using multisensor signals for robotic welding automation.[18–20]

To address these challenges, authors propose in this study a multiple-sensor-integrated framework encompassing three major components: (1) a sensor placement and control algorithm designed for optimal robotic precision using You Only Look Once (YOLO)-based visual feedback, (2) a deep-learning-based weld quality prediction model that leverages CNN and temporal attention mechanisms, and (3) a comprehensive evaluation of system performance through real manufacturing data. The proposed approach aims to enhance both the autonomy and reliability of intelligent welding systems in industrial environments.

Figure 1 shows a representative copper-tube brazing process in the household appliance manufacturing industry. In this process, a filler ring is positioned at the joint between copper tubes and heated by an induction coil to form a reliable brazed connection. Variations in tube geometry, positioning errors, or thermal disturbances can easily lead to defective brazing outcomes. This industrial context motivates the need for an integrated sensing and control framework capable of accurate target localization, robust alignment, and real-time quality assessment.

## 2. Methodology

### 2.1 Sensor deployment

To realize autonomous brazing in copper-tube joining, multiple sensors were integrated into the end-effector of a collaborative robot (Cobot). The overall configuration is shown in Fig. 2, which illustrates the complete sensing and actuation unit for the proposed system.

A thermal camera and an RGB camera were co-mounted to simultaneously capture both thermal and visual information of the brazing area. The RGB camera provides high-resolution color images that are used by the YOLO-based vision algorithm for precise object localization and robot path correction. The thermal camera monitors the temperature distribution near the brazing joint, allowing the system to evaluate heating uniformity and detect possible over- or under-heating conditions in real time.

A distance sensor is installed directly below the cameras to measure the vertical displacement between the robot tool and the copper pipe surface. This sensor enables the fine control of

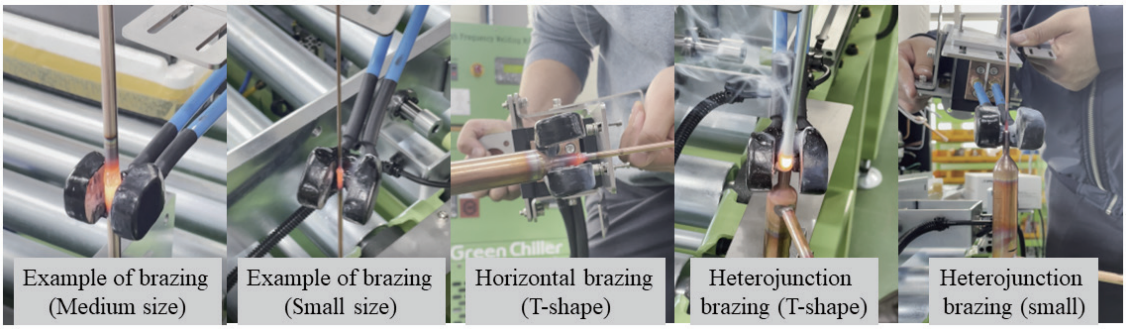


Fig. 1. (Color online) Example of copper-tube brazing application in household appliance manufacturing industry.

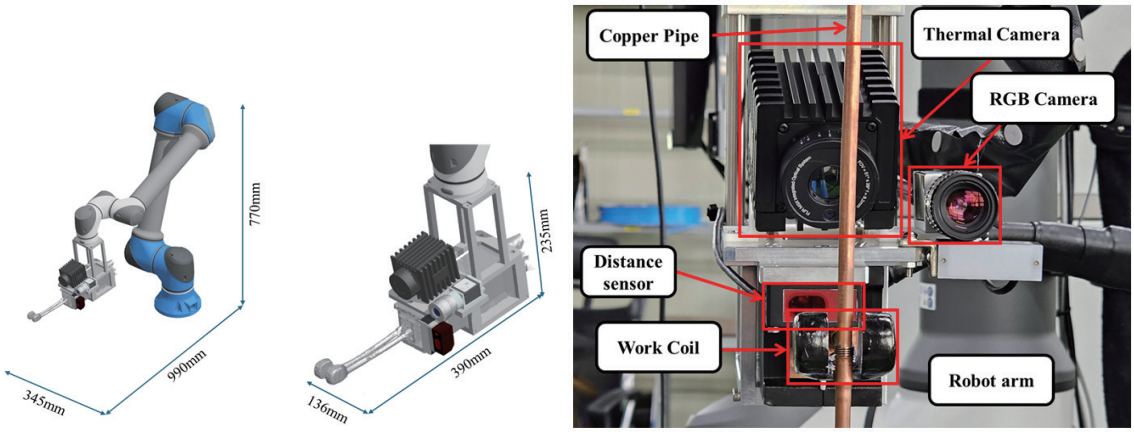


(a) (b)

Fig. 2. (Color online) Overall end-effector for Cobot copper-tube brazing application: (a) 3D overall system length and (b) sensor deployment location.

approach and standoff distance during the brazing operation. The work coil, positioned around the joint area, generates the induction heating field used for brazing. All sensors are mechanically fixed to a lightweight aluminum frame attached to the robot arm, ensuring consistent alignment and rigidity during motion.

This sensor layout was designed through empirical analysis to optimize the field of view, minimize occlusion between components, and maintain the shortest possible optical axis between the RGB camera and the thermal camera. The integrated sensing structure enables synchronized data acquisition for both control and quality assessment tasks in subsequent stages.

## 2.2 Robot control algorithm

The overall control architecture of the proposed autonomous brazing system consists of three functional layers: PC (vision and supervisor control), Robot Controller (motion control), and PLC (brazing and safety control), as summarized in Table 1.

The PC serves as the supervisory layer, executing the AI vision algorithms and generating high-level commands. It captures RGB images through the end-effector camera, performs target detection using YOLO, and calculates the target's center position and rotation angle in image

Table 1
PLC – Robot Controller – PC control system architecture.

| Device | Role | Core functions |
|---|---|---|
| PC (vision and supervision) | High-level command/AI vision | Target (filler metal) detection<br>Center, rotation angle calculation<br>Distance estimation, command generation<br>Robot control command transmission |
| Robot Controller | Motion control | Cartesian velocity/position control<br>End-effector pose computation<br>PLC/PC interface |
| PLC (brazing unit, I/O) | Sequence control | Brazing unit control, sensor signal process<br>Safety interlock, reset<br>System ready signal management |

coordinates ($u$,). On the basis of the camera calibration and system geometry, the position offset between the robot tool and the detected copper pipe is computed, producing normalized control errors for real-time motion correction. The Robot Controller interprets these commands to perform Cartesian velocity or position control while computing the precise end-effector pose required for alignment and approach maneuvers. Finally, the PLC governs the brazing unit, handling heating sequence control, sensor signal processing, and system safety interlocks. This modular configuration enables synchronized communication between all layers to achieve stable and repeatable brazing operations.

The sequential flow of the robot control process is shown in Fig. 3. After system initialization and safety checks, the robot receives alignment information and starts the operation sequence. The RGB image is captured, and the brazing target (filler metal and copper pipe joint) is detected by YOLO. The normalized positional error is calculated by comparing the detected target center ($c_x$, $c_y$) with the image center ($u$, $v$). Laser distance data are then read to determine the current depth offs*et, al*lowing the robot to adjust its vertical motion before executing the brazing command. This closed-loop process continuously updates alignment and approach parameters to ensure consistent brazing quality.

A schematic of the target detection and geometric interpretation process is presented in Fig. 4. The YOLO model identifies the bounding box of the copper pipe and computes the centroid and orientation angle of the region of interest (ROI). These image-space coordinates are then transformed into the robot coordinate frame using the pre-calibrated extrinsic parameters between the RGB camera and the end-effector. The resulting 3D offsets guide the robot's motion controller to correct its pose and achieve precise alignment before the brazing operation.

To enhance the precision of visual servoing, the positional error obtained from the YOLO detection result is converted from pixel coordinates into the real-world coordinate frame using the camera's intrinsic and extrinsic calibration parameters. Let ($u$, $v$) denote the detected target center in the image plane and ($c_x$, $c_y$) the optical center of the camera. The normalized image coordinate is computed as

$$x_n = (u - c_x) / w_{px}, \quad y_n = (v - c_y) / w_{py}, \tag{1}$$

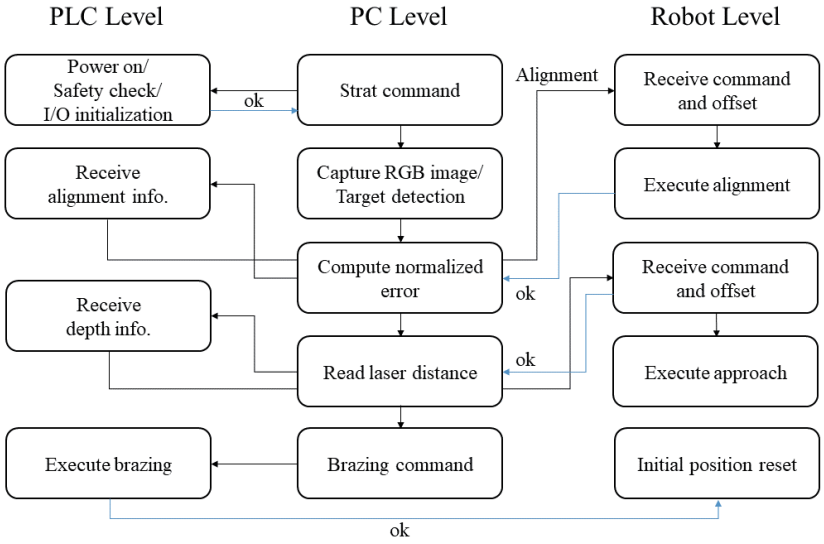


Fig. 3. Flow chart of control system architecture

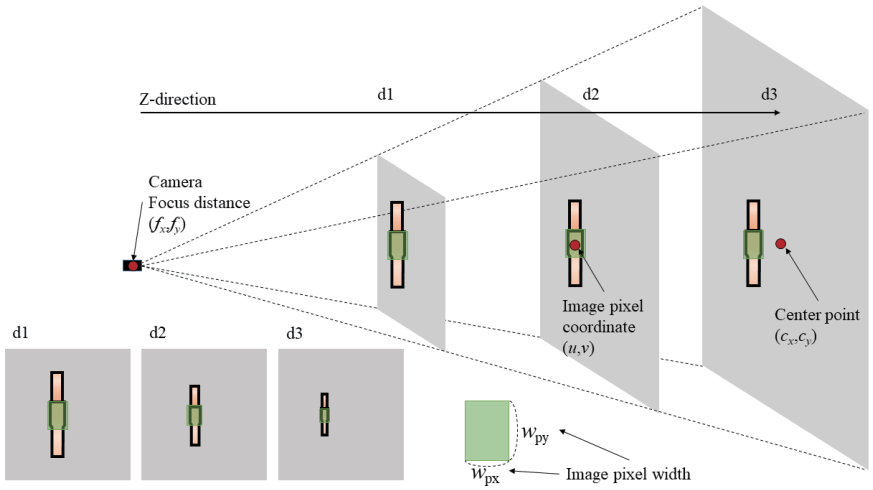


Fig. 4. (Color online) Brief structure of the YOLO architecture used for the classification of brazing target and estimation of target position and its angle.

where $w_{px}$ and $w_{py}$ represent the horizontal and vertical focal scaling factors in pixel units, respectively. These scaling factors are derived from the camera intrinsic matrix $K = [f_x\ 0\ c_x;\ 0\ f_y\ c_y;\ 0\ 0\ 1]$, where $f_x$ and $f_y$ correspond to the effective focus distance expressed in pixel units.

In monocular vision systems, the apparent positional deviation in the image plane does not linearly correspond to the real displacement of the target, since the image scale varies inversely with the depth z of the target. To compensate for this perspective distortion, a depth-normalized correction is applied using the measured distance $z_m$ obtained from the laser distance sensor. The true lateral offset ($X$, $Y$) in the camera coordinate frame is expressed as

$$X = \{(u - c_x) \cdot z_m\} / f_x, \quad Y = \{(v - c_y) \cdot z_m\} / f_y . \tag{2}$$

As the target approaches the camera, the same pixel displacement corresponds to a smaller physical error. Hence, the normalized control error ($e_x$, $e_y$) used in the robot controller is given by

$$e_x = X / z_m, \quad e_y = Y / z_m . \tag{3}$$

This normalization process effectively removes depth-induced scaling bias, ensuring that the visual servoing controller maintains consistent control gain across various working distances. By fusing real-time distance sensor feedback with vision-based offset estimation, the system achieves robust closed-loop alignment even when the copper tube height varies. This fusion approach enables depth-invariant precision control, allowing the robot to dynamically adapt its end-effector trajectory without manual recalibration, thereby improving brazing accuracy and repeatability.

### 2.3 Brazing target classification

For autonomous brazing, the accurate identification of the joint target and filler material is essential to ensure stable alignment between the copper tubes and the induction work coil. The proposed vision-based classification algorithm employs a YOLO-based deep learning detector to localize and differentiate the two primary ROIs, namely, $P_1$ (filler material) and $P_2$ (joint target), as illustrated in Fig. 5.

In this study, a YOLO-based detector (YOLO-v11-obb-n) was employed with an input resolution of 640 × 640 pixels to ensure the robust detection of elongated brazing targets such as filler materials and joint regions. The model was optimized for real-time inference on a GPU platform, enabling stable target localization and pose estimation during robotic brazing operations. The algorithm first detects the copper tube and filler material using the RGB camera mounted on the end-effector. From the bounding boxes of $P_1$ and $P_2$, the system calculates the centroid position and the relative inclination angle ($\theta$) between the filler material and the copper tube axis. This geometric relationship provides real-time feedback for robot alignment control. Specifically, the offset between the target center and the optical axis is used to correct lateral positioning, while the estimated angle $\theta$ allows the robot to adjust its rotational pose before initiating the brazing.

Through this approach, the robot can maintain precise coil placement and heating orientation, even under variations in pipe geometry or camera view angle. The YOLO-based detection model is shown schematically in Fig. 6. The network consists of three main stages: backbone, neck, and head. The backbone employs convolutional and Re-parameterized Efficient Layer Aggregation Network (R-ELAN) modules combined with flash attention layers to enhance spatial feature retention and reduce inference latency. The neck aggregates multiscale features through concatenation and upsampling operations, enabling the robust detection of both small and elongated targets such as the filler material region. Finally, the head outputs bounding boxes and

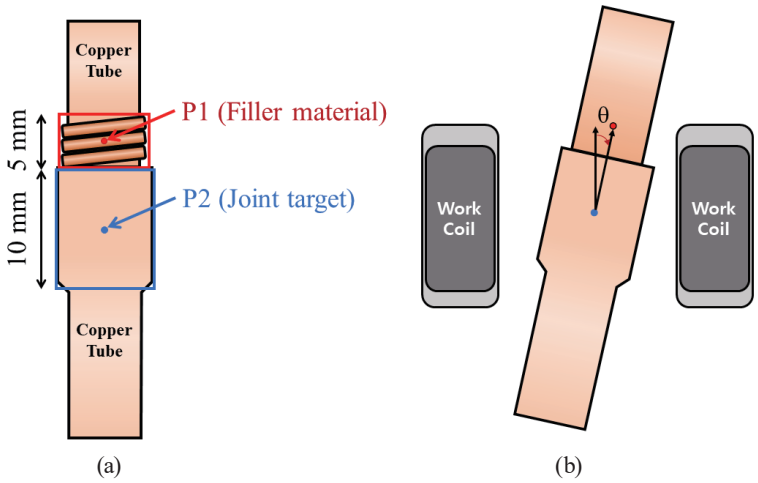


Fig. 5. (Color online) Graphical scheme of brazing targets and offset estimation: (a) filler material and joint target position and (b) estimation of angle offset.

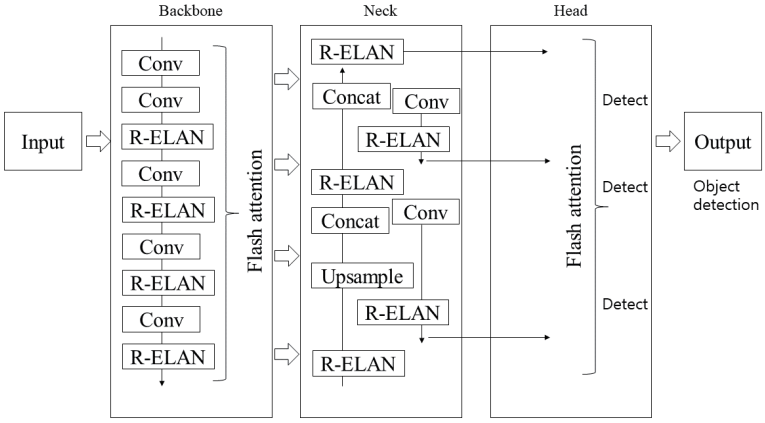


Fig. 6. Brief structure of the YOLO architecture used for the classification of brazing target and estimation of target position and its angle.

classification scores for each detected region, which are used by the controller for subsequent offset and orientation estimation. This classification module provides the fundamental perception layer in the proposed system, directly linking visual information with robotic motion control for autonomous brazing.

## 2.4 Quality inspection using CNN with temporal attention

To ensure the reliability of the brazing process, the real-time inspection of thermal patterns was implemented using a deep-learning-based spatiotemporal analysis model. During each brazing task, thermal images were continuously recorded to capture temporal changes in heat

distribution and joint formation, as illustrated in Fig. 7. The proposed model combines CNN for spatial feature extraction with a temporal attention mechanism that highlights the most informative frames across time.

The CNN encoder extracts local spatial features such as temperature gradients, heat concentration zones, and filler flow characteristics from each frame of the thermal image sequence. These features are then aggregated through a Temporal Attention Pooling layer, which assigns adaptive weights to each frame on the basis of its contribution to the overall classification task. In this way, the model focuses more on critical moments, such as the instant when the filler metal reaches its melting point or when an abnormal heat dissipation pattern occurs.

The detailed architecture of the model is summarized in Table 2. The feature extractor consists of a multistage convolutional network with progressive down-sampling and batch normalization with a fixed temporal attention window per brazing sequence. A fully connected

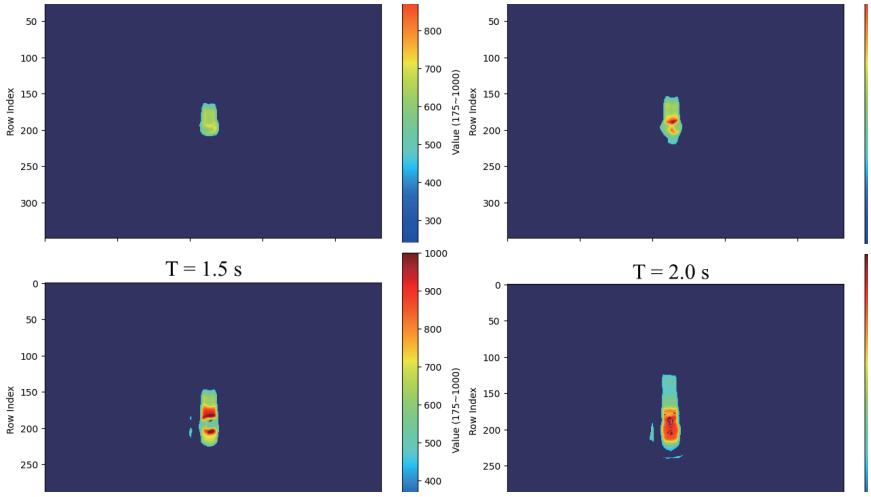


Fig. 7. (Color online) Example of historical changes in thermal image data due to brazing task.

Table 2
Model architecture of the proposed CNN-Temporal attention deep learning model.

| Component | Layer/Module | Details |
|---|---|---|
| Feature extractor | Conv2d(3→8, 7×7, stride=2, pad=3) → BN → ReLU | Input stem |
| | MaxPool2d(3×3, stride=2, pad=1) | Spatial downsampling |
| | Conv2d(8→32, 5×5, stride=2, pad=2) → BN → ReLU | Block 1 |
| | MaxPool2d(3×3, stride=2, pad=1) | Spatial downsampling |
| | Conv2d(32→64, 5×5, stride=1, pad=2) → BN → ReLU | Block 2 |
| | Conv2d(64→128, 3×3, stride=1, pad=1) → BN → ReLU | Block 3 |
| | Conv2d(128→256, 2×2, stride=1) → BN → ReLU | Head 1 |
| | Conv2d(256→512, 2×2, stride=1) → BN → ReLU | Head 2 |
| | AdaptiveAvgPool2d(output=1×1) | Global feature pooling |
| Temporal attention pooling | LayerNorm(512) + MLP(512→128→1) + GELU + Dropout(0.1) | Frame-level attention weights (softmax over time) |
| Dropout layer | Dropout ($p$ = 0.3) | Regularization |
| Classifier | Linear (512→4) | Final 4-class output |
| Total parameters | 859733 | (≈0.86 million) |

temporal attention block, implemented as a multilayer perceptron (MLP) with Rectified Linear Unit (RELU) activation and softmax weighting, computes time-dependent importance scores. The final classifier outputs four quality categories—O (Good), X (Defective), △ (Unbrazed), and XX (Failed)—with a total of ~0.86 million trainable parameters.

Thermal image sequences with a fixed temporal window of 120 frames (captured at 10 fps) were used as input to the CNN–Temporal Attention model, allowing the network to capture the full temporal evolution of heat distribution during a single brazing process. Experimental results demonstrated that this architecture achieved an $F1$-score of 98%, confirming its effectiveness in distinguishing defective brazing patterns from stable ones even under varying heating conditions. The integration of temporal attention allowed the system to detect transient anomalies that static CNNs could not capture, providing a robust approach for intelligent quality assurance in autonomous brazing systems.

## 3. Experiment

### 3.1 General conditions

To validate the proposed autonomous brazing control and quality inspection system, a series of experiments were conducted under standardized environmental and computational conditions. All experiments were performed in a controlled laboratory setup equipped with a collaborative robot and a vision-based sensing system as described in Sect. 2. The software environment was configured to ensure consistent deep learning inference and real-time data acquisition performance.

In addition, the following sensors were used for inference, detection, and measurement: an RGB camera (Basler acA3088-16gc, Germany) with a Computar M1614-MP2 lens for high-resolution visual acquisition, a thermal camera (FLIR A50 d29, USA) for real-time infrared monitoring, a direct bar illumination system (DBL-50X15, Korea) providing uniform lighting, a high-frequency induction brazing unit (10 kW, ~30 A, 15 kHz, Shin Jin Electric, Korea) ensuring stable heating, and a laser distance sensor (Panasonic HG-C1200, Japan) for the precise measurement of the gap and robot–workpiece alignment.

### 3.2 Dataset gathering

To train and validate the proposed vision-based brazing inspection model, a dataset of synchronized thermal and RGB image sequences was collected during real brazing operations.

#### 3.2.1 RGB image dataset

An RGB image dataset was constructed to train the YOLO-based brazing target detector (Yolo-v11-obb-n). A total of 803 images, including augmented samples, were collected. To improve robustness, augmentation techniques such as exposure, rotation, contrast, noise, and scaling were applied to simulate variations in lighting, viewpoint, and size. This dataset enabled

the stable detection of filler and joint targets under diverse visual conditions. To increase dataset diversity and model robustness, five augmentation techniques were applied: exposure (gamma correction), rotation, contrast adjustment, Gaussian noise addition, and scaling (zoom-out).

### 3.2.2 Thermal image dataset

A thermal image dataset was collected using a FLIR A50 d29 infrared camera to capture temperature variations during the brazing process. Thermal sequences were recorded in synchronization with RGB images, ensuring frame-level temporal alignment. Each sequence consisted of 120 frames captured at 10 fps, resulting in 12,000 thermal images from 100 brazing trials.

The dataset included four quality classes — O (41), X (21), △ (33), and XX (5) — representing different brazing outcomes. All images were preprocessed through alignment, temperature normalization, and contrast enhancement to reduce sensor noise and thermal drift. To improve robustness, six data augmentation methods (blur, noise, flip, translation, zoom, and shrink) were applied during model training. This dataset enabled the CNN–Temporal Attention model to learn temporal heat flow patterns and accurately identify defective brazing cases under various thermal conditions.

## 3.3 Learning parameters

The deep learning model was implemented and trained in a Python-based environment using the configurations summarized in Table 3.

# 4. Result

## 4.1 Brazing target classification performance

The YOLO-based detection model was trained to identify two primary brazing targets: the filler ring and the joint area. Figure 8 presents the detection results, showing both regions clearly

Table 3
General environmental setups.

| Category/parameter | Details |
|---|---|
| Python version | 3.12.10 (64-bit, MSC v.1943, AMD64) |
| Operating system | Windows 11 (10.0.26100, SP0) |
| PyTorch version | 2.7.1+cu126 |
| CUDA version | (PyTorch): 12.6 |
| CUDA available | True |
| GPU device | NVIDIA GeForce RTX 3070 |
| Learning rate | $1.0 \times 10^{-5}$ |
| Epochs | 200 |
| Batch size | 2 |
| Optimizer | Adam |
| Loss function | Cross-Entropy with label smoothing (0.02) |
| Mode | Single-split |

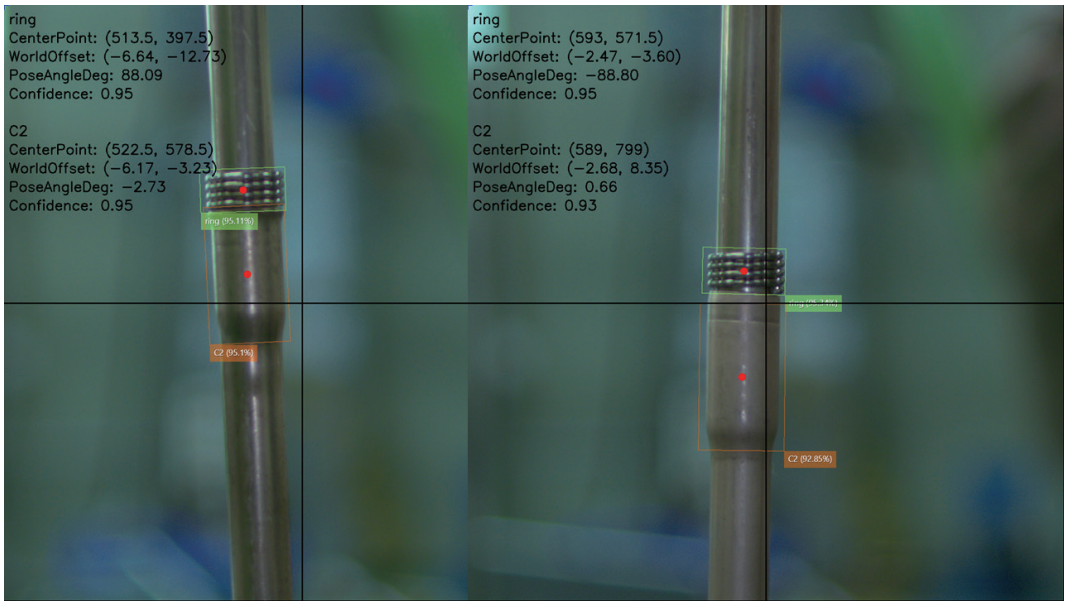


Fig. 8. (Color online) Detection results of filler and joint targets in RGB image using YOLO-based classification model.

recognized with confidence scores above 0.9, as well as their corresponding center points, world-coordinate offsets, and pose angles. These results confirm that the model successfully localizes and differentiates between the filler and joint zones under various viewing conditions.

The learning curve trends for training and validation are shown in Fig. 9. Loss values for bounding box, classification, and distribution focal loss steadily decreased throughout the training, whereas precision, recall, and mAP(50–95) metrics converged toward 0.99, demonstrating stable learning and strong generalization capability. This indicates that the proposed YOLO-based model can achieve highly accurate and consistent detection performance in real brazing applications.

### 4.2 Quality inspection performance

The proposed CNN–Temporal Attention model was trained using the thermal image dataset to evaluate brazing joint quality across four categories (O, X, △, and XX). The learning results in Fig. 10 show that both the training and validation losses rapidly converged below 0.25 within the first 10 epochs, whereas the $F1$-scores (macro and weighted) stabilized above 0.98, demonstrating effective optimization and strong generalization capability.

The class-wise $F1$-score evolution shown in Fig. 11 indicates that all four defect categories achieved stable classification performance above 0.95. Even the minority class (XX) maintained comparable accuracy, confirming that the temporal attention mechanism effectively captured time-dependent thermal features and mitigated class imbalance during learning. Overall, these results verify that the proposed model can accurately and consistently assess brazing quality under variable heating conditions.

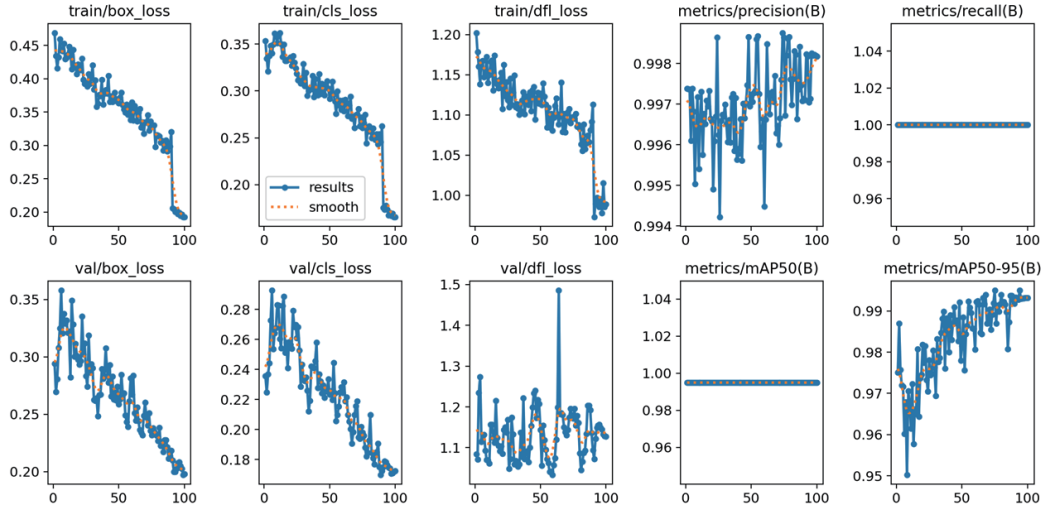


Fig. 9. (Color online) Training and validation performance of the YOLO-based brazing target detection model.

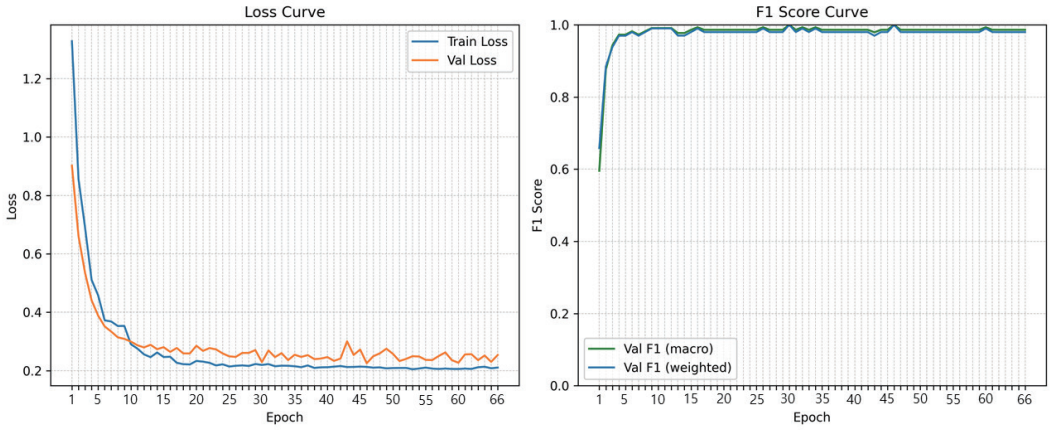


Fig. 10. (Color online) Training and validation results of the CNN–Temporal Attention model.

## 5. Discussion

### 5.1 Integration of vision and sensor feedback

The coordinated use of RGB and thermal modalities significantly improved the robustness of the robotic brazing process. The YOLO detector effectively localized filler and joint positions with sub-millimeter accuracy, maintaining a confidence score exceeding 0.9 across all conditions.

By integrating laser-based distance feedback, the control algorithm maintained stable positional correction even under various tube heights and illumination. This multisensor

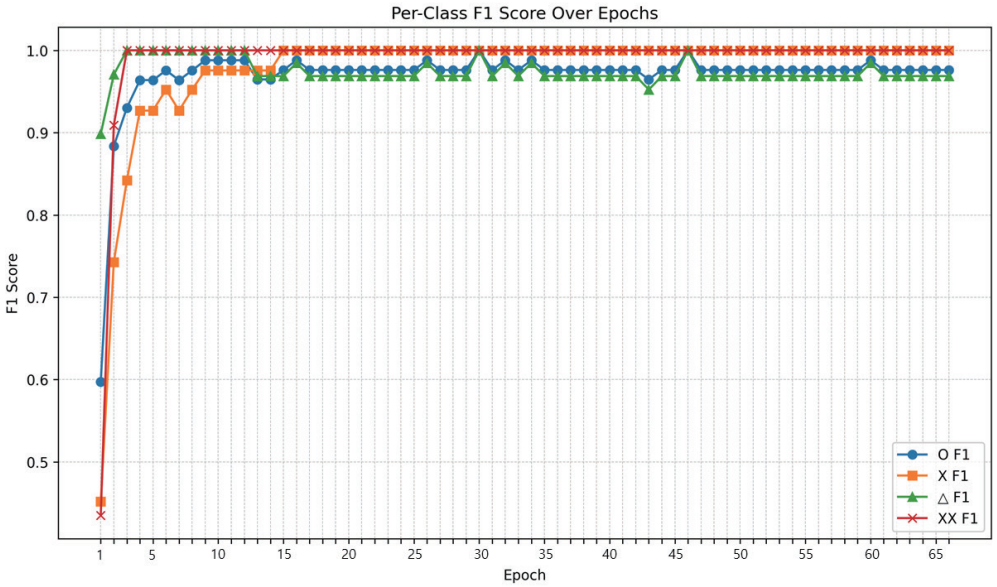


Fig. 11. (Color online) Per-class F1-score trends over epochs for the CNN–Temporal Attention model.

approach confirms the feasibility of achieving depth-invariant alignment without the need for complex 3D vision systems.

## 5.2 Temporal learning for quality estimation

The CNN–Temporal Attention model successfully captured the temporal evolution of thermal patterns during the brazing process. Unlike static frame-based classifiers, the proposed temporal pooling mechanism emphasized meaningful time-dependent features, allowing the model to distinguish between proper heating and defect formation sequences. Vision-only CNN-based inspection methods typically report $F1$-scores in the range of 0.90-0.95 under controlled conditions, while sensor-based or static thermal image classifiers show limited capability in capturing transient defect formation.[21] By explicitly modeling the temporal evolution of thermal patterns, the proposed approach achieved an $F1$-score of 0.98, indicating a clear advantage in detecting subtle and time-dependent anomalies. This behavior is consistent with related studies showing that temporal attention applied to CNN-extracted features significantly improves classification performance by learning the relative importance of time segments. Recent studies showed that attention-based temporal aggregation outperforms uniform pooling in industrial inspection and process monitoring tasks by focusing on transient but quality-critical states.[22,23] Similarly, the proposed model assigned higher attention weights to peak heat concentration and rapid thermal transitions, indicating that CNN-based temporal attention frameworks can be effectively extended to thermal image-based quality estimation in autonomous brazing systems, with strong robustness and cross-domain applicability.

### 5.3 Limitations and future work

Despite the high accuracy achieved in this study, several limitations should be acknowledged. The experimental dataset was collected under controlled laboratory conditions with fixed copper tube geometries and stable environmental settings. Variations in material type, tube diameter, surface conditions, illumination, and induction heating power may affect system performance and should be investigated in future studies. In addition, although the current framework enables real-time perception and quality assessment using GPU-based inference, fully closed-loop adaptive control, such as the automatic adjustment of brazing parameters via PLC based on predicted quality, was not implemented in this study. Future work will focus on integrating the proposed quality estimation module into a closed-loop real-time process control framework, in which the estimated quality state is fed back to the controller and used to autonomously adjust key processing parameters through rule-based or learning-based control strategies (e.g., reinforcement learning or adaptive optimization), with the goal of preventing defect formation. The proposed extension will be validated under diverse industrial operating conditions.

## 6. Conclusion

In this study, authors proposed an integrated autonomous brazing framework that combines vision-based robotic control and AI-driven quality inspection for intelligent manufacturing applications. The developed system successfully performed two primary functions: (1) precise brazing target localization using a YOLO-based RGB visual sensing algorithm, and (2) real-time defect assessment through a CNN–Temporal Attention model applied to thermal image sequences.

Experimental results demonstrated that the vision-based control system achieved sub-millimeter positioning accuracy and reliable filler–joint alignment, even under various working distances. Furthermore, the proposed deep learning inspection model achieved an overall $F1$-score of 0.98, confirming its robustness and high discriminative power across multiple defect categories.

The integration of multiple sensors—combining RGB, thermal, and laser distance data—was shown to improve process consistency and quality stability in the brazing operation. These results suggest that the proposed approach can serve as a foundation for fully autonomous manufacturing systems capable of perception, decision-making, and adaptive process control.

Future work will focus on expanding the framework toward real-time industrial deployment, including adaptive control loops with PLC–Robot synchronization and large-scale validation under diverse industrial conditions. Ultimately, the authors' work has the potential to contribute to advancing Physical AI in manufacturing, bridging the gap between automated and truly autonomous production systems.

## Acknowledgments

This work was supported by "Development of AI-based Equipment Control and Autonomous Manufacturing Operation Technology for High-quality Management of Non-standard Production Products in Home Appliance Factories" (KM-240409). The authors express their gratitude to project leader Bonggu Kim and project manager Changhoon Ryu of DH Global for his valuable support and contributions.

## References

1 K. S. W. Kim, J. H. Kong, S. W. Lee, and S. Lee: Int. J. Precis. Eng. Manuf. **23** (2022) 111. https://doi.org/10.1007/s12541-021-00600-3
2 J. Wan, X. Li, H.-N. Dai, A. Kusiak, M. Martinez-Garcia, and D. Li: Proc. IEEE **109** (2021) 377. https://doi.org/10.1109/JPROC.2020.3034808
3 S. J. Plathottam, A. Rzonca, R. Lakhnori, and C. O. Iloeje: J. Adv. Manuf. Process. **5** (2023) e10159. https://doi.org/10.1002/amp2.10159
4 A. Miriyev and M. Kovač: Nat. Mach. Intell. **2** (2020) 658. https://doi.org/10.1038/s42256-020-00258-y
5 L. Monostori: Procedia CIRP **17** (2014) 9. https://doi.org/10.1016/j.procir.2014.03.115
6 M. Pouranvari and S. P. H. Marashi: Sci. Technol. Weld. Join. **18** (2013) 361. https://doi.org/10.1179/1362171813Y.0000000120
7 J. Stavridis, A. Papacharalampopoulos, and P. Stavropoulos: Int. J. Adv. Manuf. Technol. **94** (2018) 1825. https://doi.org/10.1007/s00170-017-0461-4
8 Z. Zhang, G. Wen, and S. Chen: J. Manuf. Process. **45** (2019) 208. https://doi.org/10.1016/j.jmapro.2019.06.023
9 Y. Zhang, D. You, X. Gao, N. Zhang, and P. P. Gao: J. Manuf. Syst. **51** (2019) 87. https://doi.org/10.1016/j.jmsy.2019.02.004
10 K. Pan, H. Hu, and P. Gu: Sensors **23** (2023) 8677. https://doi.org/10.3390/s23218677
11 G. A. Elhendawy and Y. El-Taybany: Int. J. Precis. Eng. Manuf. **26** (2025) 3185. https://doi.org/10.1007/s12541-025-01281-y
12 Y. Xu and Z. Wang: Sens. Actuators, A **320** (2021) 112551. https://doi.org/10.1016/j.sna.2021.112551
13 G. Kim, Y. Kim, D. Kim, J. Park, J. Park, and J. Yu: Appl. Sci.-Basel **14** (2024) 5998. https://doi.org/10.3390/app14145998
14 J. Lu, S. Yamane, W. Wang, K. Matsutani, and Y. Luo: Int. J. Adv. Manuf. Technol. **139** (2025) 5867. https://doi.org/10.1007/s00170-025-16157-8
15 H. Sun, L. Xia, Y. Zhou, W. Qian, W. Wang, and K. Zhang: J. Manuf. Process. **129** (2024) 292. https://doi.org/10.1016/j.jmapro.2024.08.037
16 A. V. Chernov, I. K. Savvas, A. A. Alexandrov, O. O. Kartashov, D. S. Polyanichenko, M. A. Butakova, and A. V. Soldatov: Sensors **22** (2022) 8554. https://doi.org/10.3390/s22218554
17 R. Yu, T. Zhang, Y. Huang, Y. Peng, and K. Wang: Opt. Laser Technol. **184** (2025) 112432. https://doi.org/10.1016/j.optlastec.2025.112432
18 J. Wang, L. Li, and P. Xu: Sensors **23** (2023) 9700. https://doi.org/10.3390/s23249700
19 Q. Guo, Z. Yang, J. Xu, Y. Jiang, W. Wang, Z. Liu, W. Zhao, and Y. Sun: Robot. Comput.-Integr. Manuf. **89** (2024) 102767. https://doi.org/10.1016/j.rcim.2024.102767
20 T. Lei, Y. Rong, H. Wang, Y. Huang, and M. Li: Comput. Ind. **123** (2020) 103326. https://doi.org/10.1016/j.compind.2020.103326
21 M. Xiao, B. Yang, S. Wang, Z. Zhang, X. Tang, and L. Kang: Comput. Ind. **135** (2022) 103583. https://doi.org/10.1016/j.compind.2021.103583
22 X. Ma, W. Chen, Z. Pei, J. Liu, B. Huang, and J. Chen: IEEE Trans. Neural Syst. Rehabil. Eng. **31** (2023) 3188. https://doi.org/10.1109/TNSRE.2023.3299355
23 Y. Fu, C. Zhang, C. Li, M. Zhen, W. Chen, Y. Ji, and H. Hua: Electronics **13** (2024) 4889. https://doi.org/10.3390/electronics13244889